Physica E: Low-dimensional Systems and Nanostructures 115 (2020) 113681

Contents lists available at ScienceDirect

Physica E: Low-dimensional Systems and Nanostructures

journal homepage: www.elsevier.com/locate/physe

First-principles study on stability, structural and electronic properties of monolayers and nanotubes based on pure Mo(W)S(Se)$_2$ and mixed (Janus) Mo(W)SSe dichalcogenides

R.A. Evarestov*, A.V. Kovalenko, A.V. Bandura

Quantum Chemistry Department, Saint Petersburg State University, 7/9 Universitetskaya Naberezhnaya, St. Petersburg, 199034, Russian Federation

ARTICLE INFO

Keywords:
Dichalcogenide bulk crystals
Dichalcogenide monolayers
Janus MoSSe and WSSe nanotubes
Strain energy
Electronic band structure
HSE06 exchange-correlation functional

ABSTRACT

Hybrid density functional theory calculations are performed for the first time to compare the stability, structural and electronic properties of monolayers and single-wall nanotubes based on pure Mo(W)S(Se)$_2$ and mixed (Janus) Mo(W)SSe dichalcogenides. The stability, structural and electronic properties of Mo and W dichalcogenide nanotubes have been compared at different wall compositions, chiralities and diameters using the same calculation scheme. Different types of mixed nanotubes are considered – with S or Se atoms on the outer (inner) shell of the nanotube. It was found that nanotubes Se(out)WS(in) with average diameter (D_{avr}) greater than ≈ 40 Å have the negative strain energy. Our calculations show that the band gap is direct for zigzag MS$_2$ and S(out)MSe(in) nanotubes (M = Mo, W) but it becomes indirect in armchair nanotubes. For the MSe$_2$ and Se(out)MS(in) nanotubes of both chiralities, the band gap is mostly direct, except the armchair tubes with $D_{avr} < 18$ Å and zigzag tubes with D_{avr} in interval from 18 to 26 Å where it is indirect.

1. Introduction

Since the discovery of graphene [1], two-dimensional (2D) and one-dimensional (1D) materials have attracted increasing attention due to their unique properties. Strictly speaking 2D and 1D mean the dimension of the translation lattice as the materials themselves are 3D objects. In the past years 2D materials have become the main focus of research in connection with their potential use in new electronic and optoelectronic devices [2–7]. Besides the monolayer, its one-dimensional derivatives, such as nanotubes, are also considered as the promising nanomaterials for next-generation nanoelectronics [8].

Numerous 2D materials and their structural derivatives have been prepared experimentally [9–12]. Among them, the molybdenum and tungsten dichalcogenide nanolayers and corresponding nanotubes have been synthesized. For example, Tenne and his colleagues were the first who reported on the synthesis of inorganic transition metal disulfide nanotubes (NTs) based on MS$_2$ (M = Mo, W) [13]. In addition, Nath and Rao [14] obtained MoSe$_2$ and WSe$_2$ nanotubes by reducing the corresponding triselenides in hydrogen or by the decomposition of the ammonium selenometallates in a hydrogen atmosphere.

As far as we know, a mixed monolayer of MoSSe does not exist in nature, but its structure was theoretically predicted for the first time by Cheng et al., in 2013 [15], and after a short time it was successfully synthesized using the modified chemical vapor deposition (CVD) method by Lu and co-workers in 2017 [16]. To fabricate it, Lu and co-workers synthesized a monolayer of MoS$_2$ using CVD on SiO$_2$ substrate, then separated the top-layer S atoms and replaced them with H atoms using hydrogen inductively coupled plasma, and, finally, replaced H atoms with Se atoms using thermal selenization. Thus, the former up-layer S atoms in MoS$_2$ were completely replaced by Se atoms with the formation of a mixed MoSSe monolayer. Later, Kandemir and Sahin [17] studied the structural, vibrational and electronic properties of the stable WSSe single layer. In addition, they studied bilayer stacking order in the hypothetical WSSe 2H-structure.

At the present time, the mixed (Janus) nanotubes have not yet been synthesized. Nevertheless, the rapid progress in the synthesis of nanosystems allows us to hope that such an opportunity will appear in the nearest future. Theoretical modeling of these systems will undoubtedly contribute to the achievement of this goal. To date, several works have been published on the study of mixed nanotubes based on MXY (M = Mo, W; X, Y = S, Se). Among them, more attention was paid to the calculations of electronic structure and stability of mixed molybdenum dichalcogenide nanotubes, and relatively fewer works were devoted to similar tungsten dichalcogenide nanotubes. The work of Wu et al. [18] should be mentioned among the first ones. In this work [18] the electronic structure of MoXY (X, Y = S, Se) single-wall nanotubes

* Corresponding author.
E-mail address: r.evarestov@spbu.ru (R.A. Evarestov).

https://doi.org/10.1016/j.physe.2019.113681
Received 5 June 2019; Received in revised form 1 August 2019; Accepted 6 August 2019
Available online 09 August 2019
1386-9477/

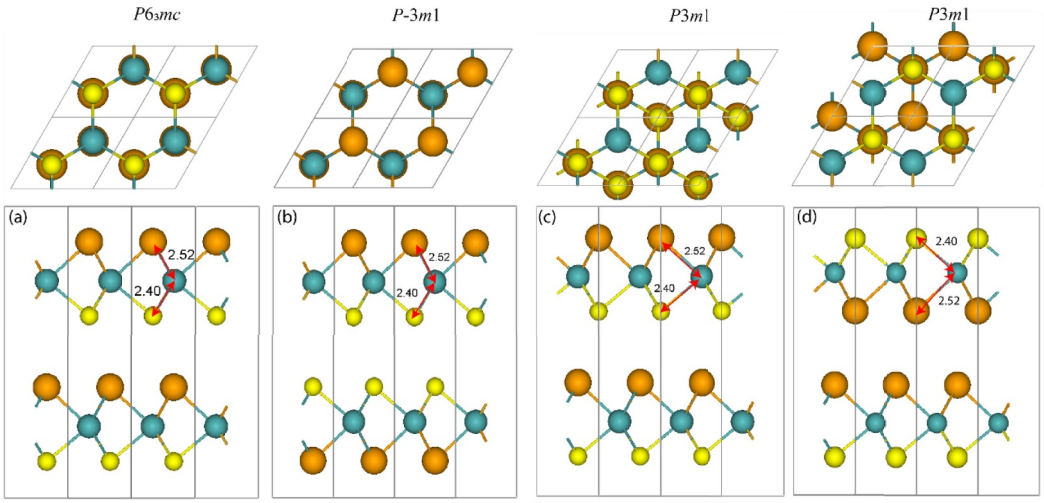

Fig. 1. Optimized structure of bulk MoSSe. View along [001] (top) and [$1\bar{1}0$] (bottom) directions, 2 × 2 × 1 cells are shown. Legend: big orange and middle yellow balls are for chalcogenides (Se and S) atoms and small blue balls are for metal atoms. (For interpretation of the references to colour in this figure legend, the reader is referred to the Web version of this article.)

Table 1
Calculated and experimental (in parentheses) properties of bulk MXY (M = Mo, W; X, Y = S, Se).

Compound	a (Å)	c (Å)	E_{atom} (eV atom^{-1})	E_{gap} (eV)	Bulk modulus (Gpa)
MoS_2	3.146	12.504	5.13	1.56	43.17(50.00 [37])
	(3.160 [35])	(12.294 [35])	(4.98 [36])	(1.29 [35])	
MoSSe	3.208	12.769	4.85	1.40	36.57
$MoSe_2$	3.268	13.087	4.59	1.36	38.07(40.78 [37])
	(3.299 [35])	(12.938 [35])		(1.09 [38])	
WS_2	3.157	12.530	5.63	1.63	44.56(52.67 [37])
	(3.153 [33])	(12.323 [33])	(5.77 [39])	(1.35 [38])	
WSSe	3.222	12.758	5.32	1.48	38.84
WSe_2	3.283	12.948	5.03	1.40	41.71(41.78 [37])
	(3.282 [33])	(12.961 [33])		(1.20 [38])	

was investigated at different NT diameters using first-principles calculations. Luo et al. in their theoretical work [19] show that the properties of mixed nanotubes depend on the composition of their inner and outer shells. In the work of Tang et al. [20], first-principles calculations of the geometry, electronic structure, and optical properties of the MoSSe nanotubes were carried out. The obtained results [20] show that the strain energy of armchair MoSSe nanotubes is noticeably less than that of zigzag nanotubes. At a radius of 21 Å, the strain energy of the armchair MoSSe nanotubes is only 0.01 eV/atom. This means that there are no energy barriers for the practical synthesis of MoSSe-based nanotubes. More important is that the calculations predict that armchair MoSSe nanotubes should exhibit good optical absorption properties in the visible light region [20].

The calculations mentioned do not analyze the possible bulk Mo (W) dichalcogenide phases to choose from them the most favorable as the reference state for further nanotubes calculations. Due to the different calculation schemes used there are some contradictions in the results obtained by different authors. In the present paper, we make attempt to overcome these difficulties with the intention of future calculations of phonon spectra and thermodynamic properties of the mixed (Janus) dichalcogenide nanotubes. In our previous work [21] we have used the hybrid density functional theory (DFT) to compare the structural and electronic properties, stability, vibrational frequencies, and thermodynamic functions of MoS_2 and WS_2-based monolayers and single-wall nanotubes using the same calculation scheme. In this article, we use a similar approach to study and compare the stability, geometry and electronic properties of mixed nanotubes MXY (M = Mo, W; X, Y = S, Se) with different composition of the inner and outer tube shells.

2. Computational details

The calculations were carried out within the framework of the DFT using the HSE06 hybrid exchange-correlation functional [22] implemented in the computer program CRYSTAL17 [23]. The Bloch one-electron functions were expressed in terms of linear combinations of atomic orbitals (LCAO). The semi-empirical Grimme correction [24] was used to account for van der Waals interactions. As in our previous works [21,25,26], Conesa approach [27] was applied to evaluate Grimme dispersion correction parameters. The interaction between core electrons and valence and sub-valence electrons in Mo and W atoms and between core and valence electrons in the S and Se atoms was described by means of the CRENBL [28–31] relativistic effective core pseudopotentials. The corresponding Gaussian basis sets were used in calculations. The Monkhorst-Pack method was applied [32] to generate **k**-points for Brillouin zone (BZ) sampling. The **k**-point meshes with shrinking factors 18 × 18 × 6, 18 × 18, and 18 were used for hexagonal bulk, monolayer, and nanotubes, respectively. The Kohn-Sham equations were solved iteratively before self-consistency within the total energy range of 10^{-8} eV. The lattice constants and the positions of all atoms were fully optimized until forces acting on the atoms became below the value of 0.003 eV Å^{-1}.

3. Bulk and monolayer properties: comparison between MXY (M = Mo, W; X, Y = S, Se)

At the first stage of our investigation, we calculated the properties of 2H-polytypes of bulk molybdenum and tungsten dichalcogenides. It is known [33,34] that the most stable bulk MS_2 and MSe_2 (M = Mo, W)

Table 2
Calculated and experimental (in parentheses) properties of monolayers MXY (M = Mo, W; X, Y = S, Se).

Compound	a (Å)	M-S (Å)	M-Se (Å)	E_{form} (eV)	E_{atom} (eV/atom)	E_{gap} (eV)
MoS_2	3.148 (3.150 [40])	2.40	–	0.24	5.05	2.33 (1.80 [41])
MoSSe	3.207 (3.252 [42])	2.40 (2.41 [16])	2.52 (2.58 [16])	0.26	4.76	2.23
$MoSe_2$	3.267 (3.320 [43])	–	2.52	0.27	4.50 (4.56 [43])	2.11 (1.55 [44])
WS_2	3.161	2.41	–	0.23	5.64	2.53(2.05 [45])
WSSe	3.223	2.41 (2.42 [17])	2.52 (2.54 [17])	0.27	5.23	2.41
WSe_2	3.286	–	2.53	0.30	4.93	2.27

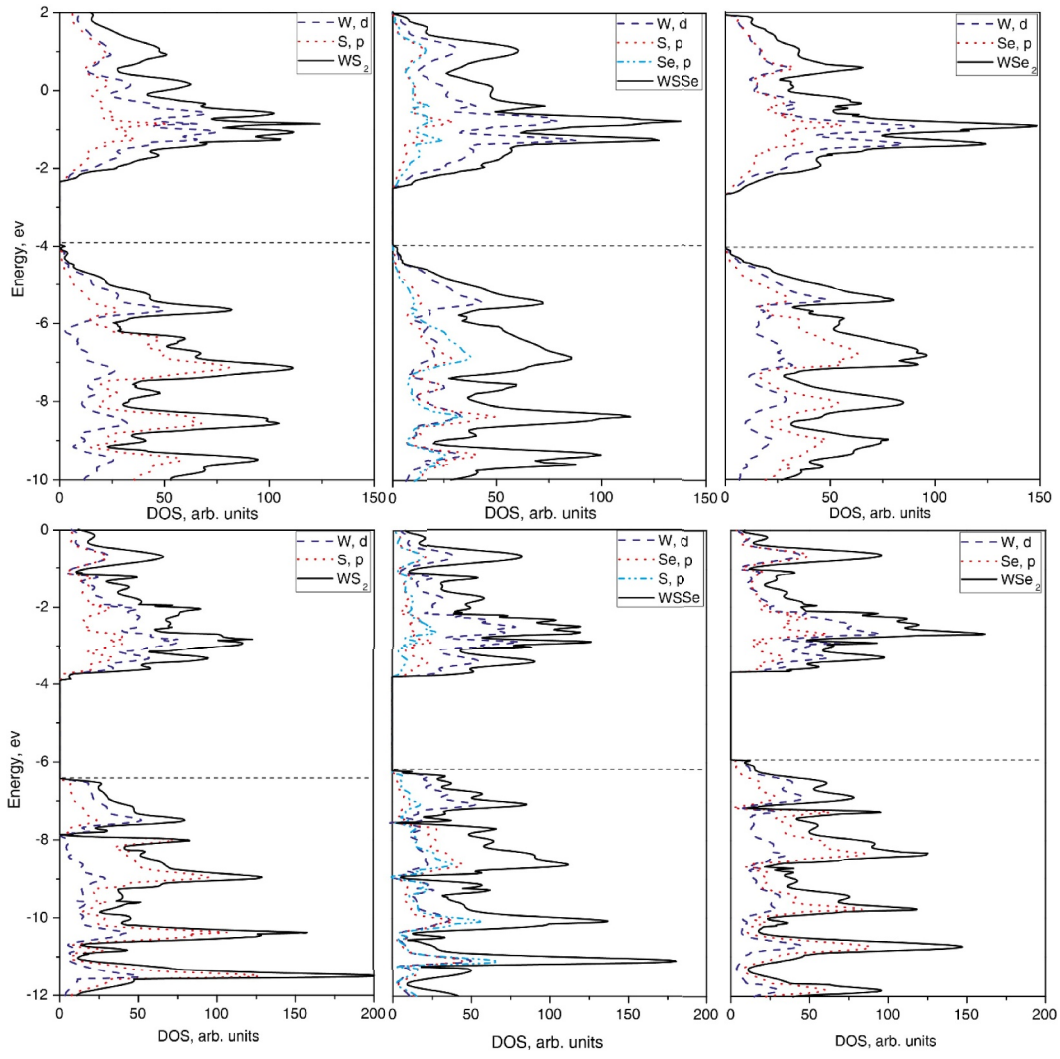

Fig. 2. Total and projected density of states of bulk phases (top) and monolayers (bottom) of (from left to right) WS_2, WSSe and WSe_2. Fermi level is shown as the horizontal dashed line.

have a hexagonal layered structure with the space group $P6_3/mmc$. The primitive unit cell consists of two triple-plane monolayers which are stacked together with weak van der Waals interactions. In hexagonal monolayers the S (Se) atoms are positioned in trigonal-prismatic coordination around the metallic atoms. In the mixed monolayer the one of S (Se) atomic plane is replaced by alternate Se (S) atomic plane. The properties of pure (unmixed) bulk phases have been studied in a number of theoretical works including our previous investigations of MoS_2 and WS_2 [21,25].

Taking into account the results of the previous simulations [17] of the mixed bilayer, we constructed the four hypothetical structures of bulk MSSe (M = Mo, W) phases. They have a hexagonal layered structure with space group $P6_3mc$ (for the first one), $P\text{-}3m1$ (for the second one), and $P3m1$ (for the last two ones). The calculated structures of MoSSe polytypes is shown in Fig. 1. According to our calculations, the third structure with the space group $P3m1$ (Fig. 1c) has the lowest energy (see Table S1 in Supplementary Material). It corresponds to a bilayer type AA′ in the classification used by Kandemir et al. [17]. We consider this structure as the most probable for the mixed bulk phase and all data below are given only for it.

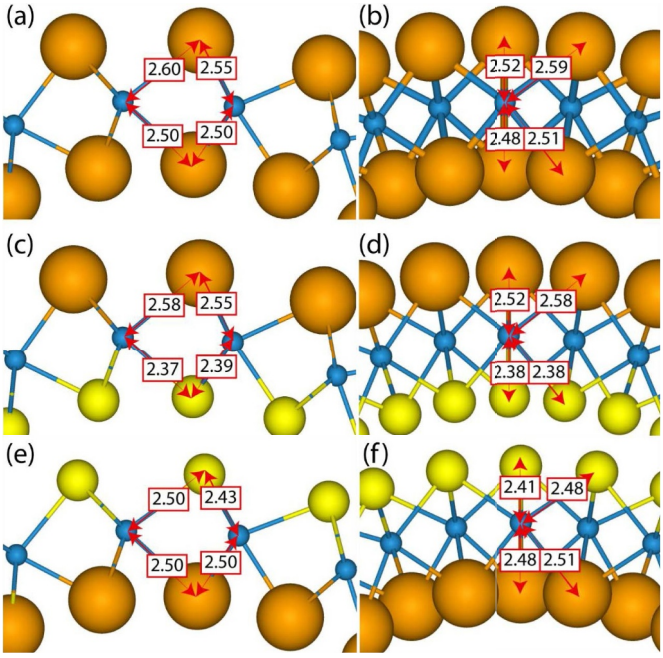

Fig. 3. Fragmentary cross-sectional view on the optimized structures of WSe_2 (a–b), SeWS (c–d) and SWSe (e–f) (12, 12) nanotubes (left) and (20, 0) nanotubes (right) with similar $D_{avg} \approx 22$ Å. The specified Mo–S and Mo–Se bond lengths are in Angstrom units. Calculated W–S and W–Se bonds lengths in the relaxed monolayers are 2.41 Å and 2.53 Å, correspondingly(seeFig. 1 for atom labeling).

Table 3
Calculated structure of nanotubes MXY (M = Mo, W; X, Y = S, Se). (D_{avg} – average diameter NT, L – period of nanotube, w – nanotube wall thickness).

Chirality	$MoSe_2$			SeMoS			SMoSe		
	D_{avg}, Å	L, Å	w, Å	D_{avg}, Å	L, Å	w, Å	D_{avg}, Å	L, Å	w, Å
(6,6)	12.06	3.30	3.14	11.54	3.24	3.09	11.91	3.23	3.00
(12,12)	22.36	3.28	3.28	21.68	3.22	3.20	22.05	3.22	3.16
(18,18)	32.93	3.27	3.31	32.08	3.21	3.23	32.47	3.21	3.20
(10,0)	12.11	5.42	3.13	11.64	5.32	3.08	11.83	5.39	3.00
(20,0)	21.85	5.60	3.28	22.17	5.50	3.21	22.46	5.52	3.16
(30,0)	31.94	5.62	3.31	31.09	5.53	3.23	31.45	5.53	3.20
Chirality	WSe_2			SeWS			SWSe		
	D_{avg}, Å	L, Å	w, Å	D_{avg}, Å	L, Å	w, Å	D_{avg}, Å	L, Å	w, Å
(6,6)	12.05	3.33	3.13	11.54	3.27	3.08	11.91	3.25	3.00
(12,12)	22.46	3.30	3.28	21.77	3.24	3.20	22.13	3.24	3.16
(18,18)	33.11	3.30	3.31	32.23	3.23	3.23	32.62	3.23	3.20
(10,0)	12.06	5.50	3.13	11.62	5.39	3.08	11.80	5.44	3.00
(20,0)	21.91	5.64	3.27	22.23	5.54	3.20	22.54	5.55	3.16
(30,0)	32.09	5.67	3.31	31.22	5.56	3.23	31.57	5.56	3.20

After geometry optimization, the atomization energy (E_{atom}) and the band gap (E_{gap}) were calculated for bulk crystals. Obtained results, together with the available experimental values, are given in Table 1. It can be seen that the calculation method used in this work provides the lattice parameters and physical properties of bulk MX_2 (M = Mo, W; X = S, Se) pure phases in good agreement with known experimental data, although the estimation of lattice constant c is less precise than the estimation of lattice constant a.

At the second stage of our study, the monolayers of MXY (M = Mo, W; X, Y = S, Se) were simulated. The monolayer formation energy (E_{form}) was calculated according to the following formula:

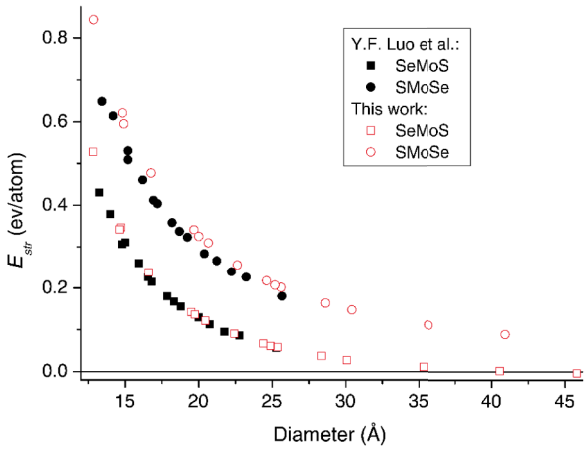

Fig. 4. Diameter dependence of strain energies of MoSSe-based nanotubes (with both considered chiralities).

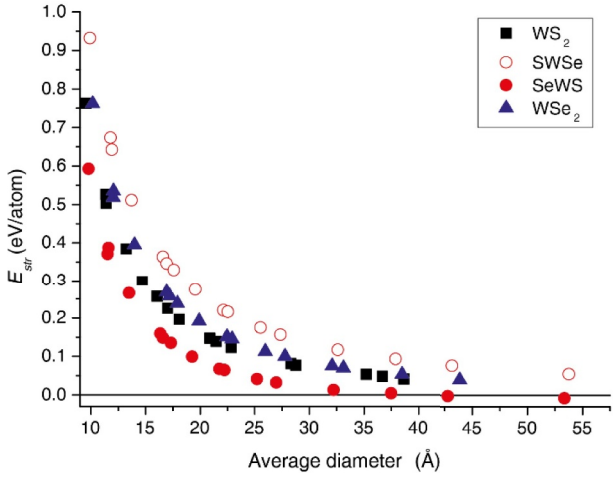

Fig. 5. Diameter dependence of strain energies of WXY (X, Y = S, Se) nanotubes (with both considered chiralities).

$$E_{form} = \frac{E_{slab}}{n_{slab}} - \frac{E_{bulk}}{n_{bulk}} \quad (1)$$

where E_{slab}, n_{slab} and E_{bulk}, n_{bulk} are the total energy and the number of formula units in monolayer and bulk unit cells, correspondingly.

Table 2 shows the following calculated properties of monolayers: the lattice constant a, the M-S(Se) bond lengths, the formation energy E_{form}, the atomization energy E_{atom}, and the band gap E_{gap}. It can be seen that the lattice constant a and the formation energy E_{form} increases in the series MS_2 < MSSe < MSe_2 (M = Mo, W), but the band gap E_{gap} decreases in this series. The M-S and M-Se bond lengths in the MSSe compounds (M = Mo, W) are practically equal to the corresponding bond lengths in the MS_2 and MSe_2 pure monolayers.

Fig. 2 shows the total density of states (DOS) and projected density of states (PDOS) of the bulk phases and triple-plane WXY (X, Y = S, Se) monolayers. It is seen that total DOSs of the bulk and monolayer valence band (VB) can be divided in two sub-bands. VB bottom states form a wide sub-band with the dominant contribution of p-orbitals of chalcogen atoms. VB top states have a greater contribution of d-orbitals of metal. A narrow minimum between VB top and bottom states is more pronounced in the monolayer DOSs. In the case of WSe_2 monolayer, the Fermi level is higher than that in WSSe and WS_2 monolayers. In the LCAO calculations of 1D and 2D systems the Fermi level is referenced to a vacuum. Our results clearly show that the VB maximum rises in the sequence: WS_2 < WSSe < WSe_2, thus providing the reducing of band

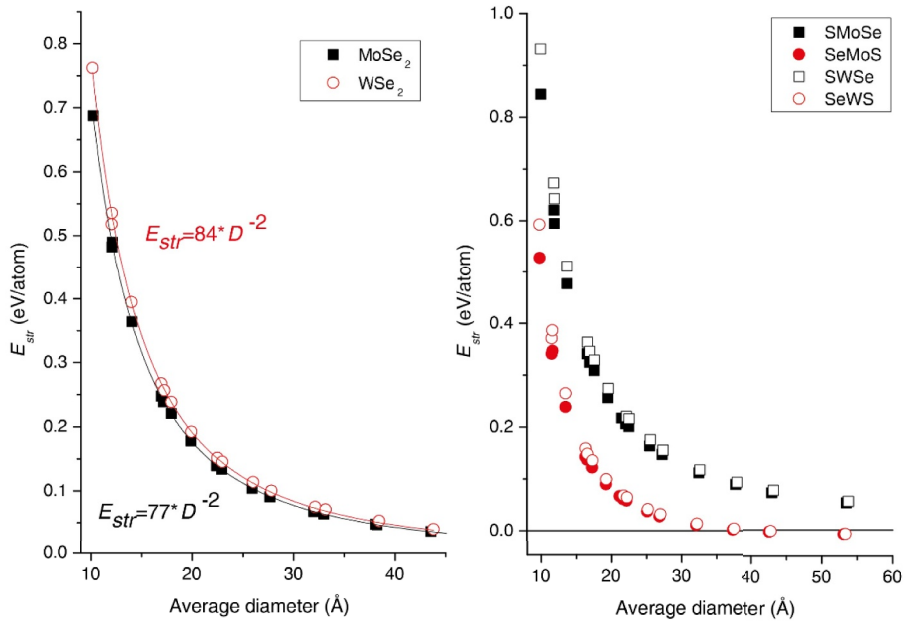

Fig. 6. Diameter dependence of strain energies of MSe_2-based nanotubes (left) and MSSe-based nanotubes (right) (M = Mo, W). Both considered chiralities are included.

Table 4
Band structure evolution of WSe_2 nanotubes.

Chirality	(6, 6)	(12, 12)	(15, 15)	(24, 24)	(8, 0)	(16, 0)	(18, 0)	(24, 0)	(30, 0)
D_{avg}, Å	12.05	22.46	27.77	43.86	10.15	17.91	19.90	25.96	32.09
E_{gap}, eV	0.57	1.78	2.06	2.18	0.39	1.44	1.64	1.85	2.11
Band gap	**indirect**	**indirect**	direct	direct	direct	direct	**indirect**	**indirect**	direct

gap (BG) in the same sequence. Molybdenum dichalcogenides exhibit the same DOS picture as tungsten dichalcogenides both for bulks and monolayers (see Fig. S3 in Supplementary Material).

4. Comparison of the structure, stability and electron properties of MXY (M = Mo, W; X, Y = S, Se) nanotubes

We performed the calculations of armchair (n, n) and zigzag (n, 0) MXY (M = Mo, W; X, Y = S, Se) achiral nanotubes, which were generated by rolling up of the corresponding pure and mixed monolayers. We consider armchair nanotubes with n = 6–30 and zigzag nanotubes with n = 8–30. The diameters of these nanotubes lay between 10 Å and 54 Å. The average NT diameters D_{avg} have been estimated as a sum of r_{in} and r_{out} which are the distances from inner and outer chalcogen atom centers to a tube axis, respectively. During optimization we keep the full NT line group symmetry including the rotohelical symmetry operations. Because of this, all NT atoms are located on the surfaces of three cylinders (shells) nested into each other, and r_{in} and r_{out} are the same for all inner and outer atoms. In the case of MSSe (M = Mo, W) nanotubes, the outer (inner) atomic shells can be different (composed of S or Se atoms), which leads to the different composition of the tube surface, its structure and, furthermore, different NT electronic properties. We will designate by SMSe the nanotube, in which the sulfur atoms form the outer shell and selenium atoms form the inner shell, and by SeMS – the opposite case.

In Fig. 3 we show the relaxed structure of XMoY (X, Y = S, Se) nanotubes with chiralities (12, 12) and (20, 0) which have approximately the same diameters of about 22 Å. When the monolayer is rolled up to a nanotube, one X-plane (X = S, Se) becomes the outer shell and another – the inner shell. Folding the monolayer into a nanotube induces the elongation of the lengths of external W–S (Se) bonds directed mainly across the tube axis by about 0.02–0.07 Å (see Fig. 3). On the contrary, the internal bonds W–S (Se) shrink by 0.02–0.04 (0.02–0.05) Å. External bonds aligned mainly with the tube axis are slightly lengthened or shortened in armchair or zigzag NTs, respectively. Evidently, with tube diameter increasing, bond lengths gradually return to values in a monolayer.

The period of nanotubes (n, 0) is about 3.2–3.3 Å, and it is about 5.3–5.6 Å for nanotubes (n, n) which is close to the initial values before optimization (the initial period of (n, 0) NT is equal to monolayer lattice constant, while the initial period of (n, 0) NT is $\sqrt{3}$ times larger). However, the period of zigzag nanotubes reduces, whereas the period of armchair nanotubes enlarges with NT diameter increasing (see Table 3). The NT wall thickness w increases and tends to the thickness of the monolayer when the diameter rises. The wall thickness of nanotubes with selenium in the inner shell is less than that of nanotubes with sulfur in the inner shell. This is especially noticeable for nanotubes with small diameters. When molybdenum is replaced with tungsten, the period of similar nanotubes slightly increases while the other NT parameters remain practically unchanged.

The stability of the nanotube can be measured by so called strain energy E_{str}, that is, the formation energy (per formula unit) of the nanotube from the monolayer:

$$E_{str} = \frac{E_{NT}}{n_{NT}} - \frac{E_{slab}}{n_{slab}} \quad (2)$$

where E_{NT}, n_{NT} and E_{slab}, n_{slab} are the total energy and the number of formula units in nanotube and monolayer unit cells, correspondingly.

Comparison of energies calculated for molybdenum dichalcogenide nanotubes shows a large difference between the strain energies of SeMoS and SMoSe for a given diameter, namely, the SeMoS is more favorable than SMoSe. This is in accordance with the results of the

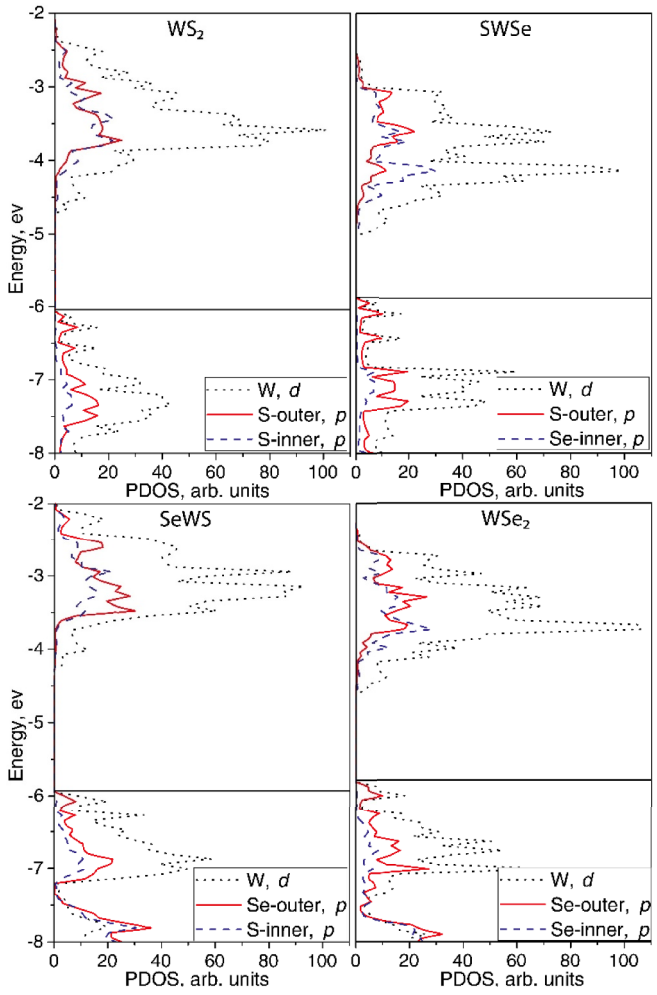

Fig. 7. Projected density of states of WS_2, SWSe, SeWS and WSe_2 nanotubes with chirality (9, 9). Fermi level is shown as the horizontal line.

previous plane-wave DFT PBE calculations: Luo et al. [19] and Tang et al. [20]. In Fig. 4, we compare E_{str} calculated by us and those obtained with the PBE functional in the mentioned study. As one can see, the data of Luo et al. [19] for SMoSe are somewhat lower than ours for a given NT diameter, whereas there is practically no difference for SeMoS NTs. Here, for the case of comparison we used the relation $D = 2*r_{in}$, where r_{in} are the radii from the center to the inner shell because this particular definition of NT diameter was used in the previous work [19]. In contrast to results of Tang et al. [20] and in accordance with results of Luo et al. [19] we did not find a noticeable difference in diameter dependence of the strain energies of armchair and zigzag MoSSe nanotubes.

Our data show that nanotubes SeMoS at D_{avr} greater than approximately 40 Å have the negative strain energy. As a result, the strain energy has a minimum at diameters of ≈75 Å (see Fig. S4 in Supplementary Material). This behavior of E_{str} is similar to that for halloysite and imogolite (aluminosilicate) single-wall or double-walled nanotubes [46,47], which were actually synthesized and also have different composition of the inner and outer surfaces.

In Fig. 5 we compare the calculated strain energies E_{str} of the pure and mixed WXY (X, Y = S, Se) nanotubes with different S/Se locations for the both considered chiralities (n, n) and (n, 0). As one can see, the strain energies of SeWS nanotubes with inside sulfur atoms are smaller than the strain energies of SWSe nanotubes with outside sulfur atoms as it was found for MoXY NTs. For small diameters, the strain energies of WSe_2 nanotubes are slightly higher than E_{str} of WS_2 nanotubes, whereas this difference becomes insignificant at large diameters. Similar to SeMoS, the nanotubes SeWS have the negative strain energy at $D_{avr} > 40$ Å. At a fixed diameter, E_{str} increases in the following order: SeWS < WS_2 ≤ WSe_2 < SWSe. The difference between E_{str} of SeWS and SWSe nanotubes is noticeably greater than the difference between E_{str} of WS_2 and WSe_2 nanotubes. This result can be easy explained by the fact that the location of larger Se atom inside the nanotube opposes the monolayer folding, whereas the alternate location promotes it.

In Fig. 6, we compare the strain energies E_{str} of the MoXY (X, Y = S, Se) nanotubes with those of the WXY (X, Y = S, Se) nanotubes. As one can see, the strain energies of the WSe_2 nanotubes are slightly higher than the strain energy values of the $MoSe_2$ nanotubes at small diameters, whereas the difference becomes insignificant at large diameters. The calculated strain energies are approximately proportional to $1/D^2$ as predicted by the classical theory of elasticity [48].

Among the electronic properties of nanotubes under consideration, we have calculated the band structure and density of states. According to data in Table 4, the band gap of WSe_2 nanotubes increases monotonically with diameter increasing. For small diameter armchair nanotubes the band gap is indirect, but it becomes direct when the diameter increases. This phenomenon is also specific to SeMoS and SeWS nanotubes (see Table S5 in Supplementary Material). For zigzag nanotubes, the band gap is direct, while for nanotube with n = 18–24 it becomes indirect. With a further diameter increase, the direct band gap is returned. Wu et al. [18] also observed this effect of indirect-direct band gap crossover for molybdenum dichalcogenide nanotubes. Also, Gao et al. [49] found that the armchair WSe_2 nanotubes have the indirect (direct) band gap when $n \leq 15$ ($n > 15$), while the zigzag ones always possess a direct band gap regardless of n.

In the work of Luo et al. [19], the band structure was calculated for mixed armchair nanotubes with n = 5–12 and zigzag nanotubes with n = 9–18. The results [19] show that armchair MoSSe nanotubes are mainly indirect semiconductors, while zigzag ones are mostly direct semiconductors. The nanotubes with S-outer layers have much smaller band gaps than the ones with Se-outer layers. In the work of Wu et al. [18], the MoS_2 armchair nanotube demonstrates an indirect band gap depending on nanotube diameters from 10 Å to 50 Å, while MoSSe and $MoSe_2$ exhibit a surprising diameter-induced indirect–direct band gap crossover at the diameters of 25 Å and 33 Å, respectively.

To analyze changes in electron states near the valence band maximum and conduction band minimum due to layer folding, we have calculated the PDOS of W d-orbitals and S (Se) p-orbitals located in the inner or outer shells of selected nanotubes. Calculated PDOS is displayed in Fig. 7; to improve the visibility of the curves, we smoothed them. It can be seen that states near the top of VB and bottom of CB mainly consist of W d-orbitals, while below and above these states the larger contribution of chalcogenide p-orbitals takes place. The PDOS analysis also shows that in all cases the contribution of S (Se)-outer p-orbitals to the top VB states is greater than contribution of S (Se)-inner p-orbitals. In the cases of SWSe and WS_2 nanotubes it is comparable to that of W d-orbitals. As the diameter increases, the contribution of the inner shell increases (see Figure S8 in Supplementary Material). Thus, we can suppose that it is the composition of the outer shell that determines the peculiarities of the band gap dependence on tube diameter.

We found that in accordance with conclusion above, the dependence of the band gap of SWSe nanotubes on the diameter is similar to that of WS_2 nanotubes, and the dependence of BG of SeWS nanotubes is similar to that of BG for WSe_2 nanotubes. The fundamental BG increases with the tube diameter in all cases. At equal diameters the band gaps of zigzag and armchair WS_2 and SWSe nanotubes are close to each other (see Fig. 8a). However, the diameter plays a more pronounced role for WSe_2 and SeWS nanotubes (see Fig. 8b and c).

The inverse relation between the band gap of cylindrical SWNTs and the tube diameter was found in some previous works [21,50,51]. We applied this approach to illustrate the differences between dichalcogenide nanotubes. The obtained dependences are shown in Fig. 8 for

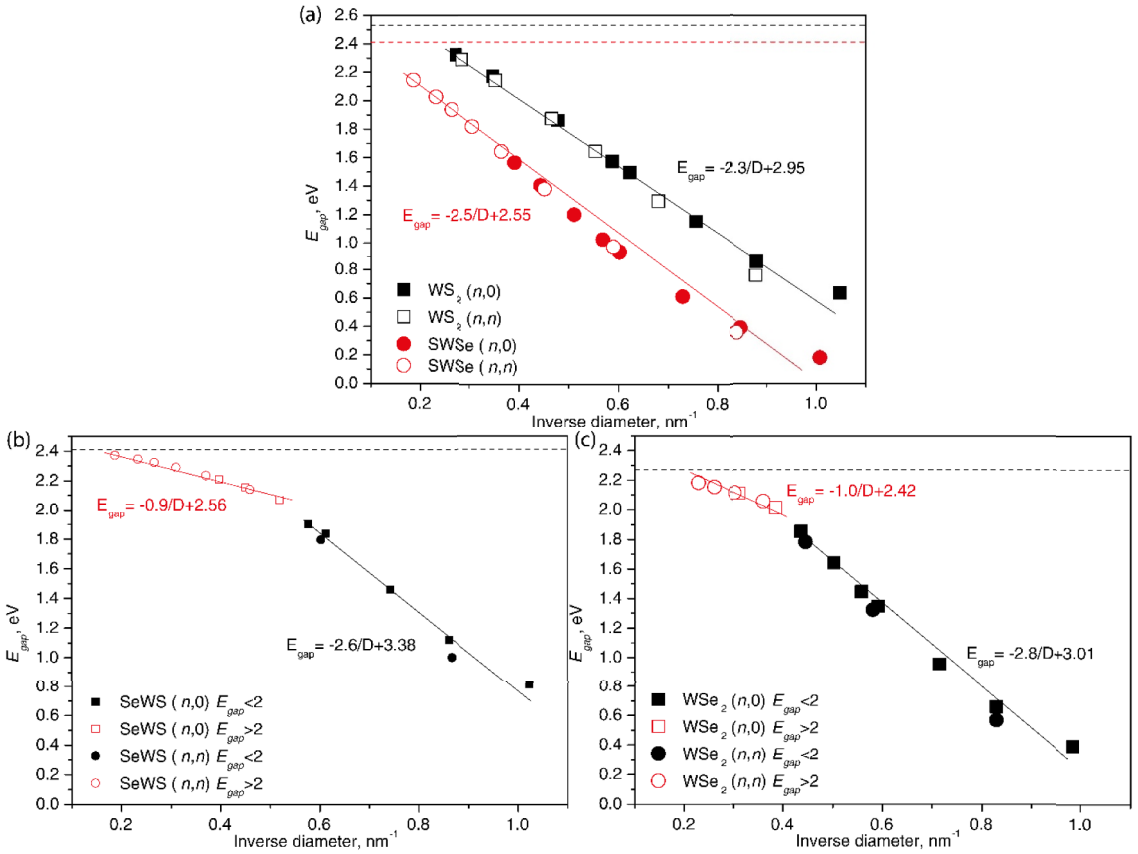

Fig. 8. Inverse diameter dependence of band gap for zigzag and armchair WS_2 and SWSe NTs (a), for SeWS NTs (b), and for WSe_2 NTs (c). Band gap of monolayer is shown as the horizontal dotted line.

considered nanotubes of both chiralities. As can be seen, the data for both the WS_2 and SWSe nanotubes are well approximated by a single line. The limiting values at $D \rightarrow \infty$ ($1/D = 0$) are 2.95 and 2.55 for the WS_2 and SWSe nanotubes, respectively. Band gaps for SeWS and WSe_2 nanotubes can be divided into two zones: when the calculated $E_{gap} < 2$ eV and $E_{gap} > 2$ eV. The fitted lines have a different slope in those two regions. In the second region the limiting values are 2.56 and 2.42 for the SeWS and WSe_2 nanotubes, respectively. Obtained limiting values are slightly above the band gaps in corresponding monolayers.

Obviously, diameter dependence of BG has its origin in the diameter-dependent curvature of the X-M-Y triple layers. It is accompanied by compressive and tensile strain in the inner and outer part of one triple layer, respectively, whose magnitude again depends strongly on the curvature (which is proportional to $1/D$) of the rolled layers and hence on the diameter D of the tube wall as a whole. As it was argued in Refs. [52,53], the main reason for the band gap shrinking lies in the tensile strain that brings down the conduction band's antibonding Mo-*d*-S-*p* states near the K point. The $1/D$ low may be due to the fact that the tensile strain is equal to w/D, where w is the thickness of the NT wall.

5. Conclusions

In summary, we have theoretically investigated a series of MXY (M = Mo, W; X, Y = S, Se) bulk crystals, monolayers and single wall nanotubes using DFT calculations. To find out the ground bulk state for mixed (Janus) systems, we modeled four hypothetical structures for the MSSe (M = Mo, W) bulk crystals. We obtained the similar optimized bulk lattice parameters for all the unit cells considered. The structure with the space group *P*3*m*1 appears to be the most stable. The unit cell of this structure consists of two three-plane MSSe layers, with the different composition (S or Se) of opposite atomic planes, separated by a vacuum gap. The knowledge of the structure and stability of mixed dichalcogenide bulk crystals could be useful for the interpretation of properties of mixed (Janus) multi-walled nanotubes.

Currently, the mixed nanotubes have not yet been synthesized, and one can hope that a theoretical modeling of these systems will facilitate their successful synthesis in the nearest future. To this purpose, we studied the dependence of stability, structural and electronic properties of Mo and W dichalcogenide nanotubes on their composition, chirality and diameter. Using the unified approach and the same calculation scheme allows us to perform a comparison between properties of pure and mixed (Janus) systems. In accordance with the previous results we show that the strain energy increases in the following order: SeMS < MS_2 < MSe_2 < SMSe (M = Mo, W). The energy advantage of SeMS nanotubes compared to SMSe nanotubes is because the location of larger Se atom inside the nanotube opposes the monolayer folding, whereas the alternate location promotes it. At the same time, there is no significant difference between the strain energies of armchair and zigzag nanotubes at equal diameters. Replacement of tungsten with molybdenum does not affect the strain energy of nanotubes. Comparing to the previous works [18–20] we considered the larger scope of NT chiralities, diameters and compositions. We more carefully analyzed the dependences of NT stability and electronic properties on diameter. Thus, we found that the nanotubes SeMS at $D_{avr} > 40$ Å have the negative strain energy that is very meaningful for the practical synthesis of these nanotubes. The minimum strain energy was located at approximately 75 Å.

Our calculations show that the band gap is direct for zigzag MS_2 and SMSe (M = Mo, W) nanotubes but it becomes indirect in armchair nanotubes. For the MSe_2 and SeMS nanotubes of both chiralities, the band gap is mostly direct, except the small diameters for armchair tubes and within the diameter interval from 18 to 26 Å for zigzag tubes where

it is indirect. The band gap dependence on diameter and the PDOSs analysis show that SMSe nanotubes are similar to the MS_2 nanotubes while the SeMS nanotubes are similar to the MSe_2 nanotubes (M = Mo, W). We proved that in the case of SeMS and MSe_2 nanotubes the band gap diameter dependence can be divided into two zones. Thus, we can propose that the composition of the outer atomic shell determines the electronic properties and peculiarities of the band gap dependence on tube diameter. The possible reason is that it is the tensile strain of outer NT shell may govern the value of nanotube band gap.

Conflicts of interest

There are no conflicts to declare.

Acknowledgments

The authors acknowledge the financial support provided by the Russian Foundation for Basic Research (Grant No. 17-03-00130-a) and the assistance of the University Computer Center of Saint-Petersburg State University in the accomplishment of high-performance computations.

Appendix A. Supplementary data

Supplementary data to this article can be found online at https://doi.org/10.1016/j.physe.2019.113681.

References

[1] K.S. Novoselov, Electric field effect in atomically thin carbon films, Science 306 (2004) 666–669, https://doi.org/10.1126/science.1102896.
[2] Q.H. Wang, K. Kalantar-Zadeh, A. Kis, J.N. Coleman, M.S. Strano, Electronics and optoelectronics of two-dimensional transition metal dichalcogenides, Nat. Nanotechnol. 7 (2012) 699–712, https://doi.org/10.1038/nnano.2012.193.
[3] C. Tan, X. Cao, X.-J. Wu, Q. He, J. Yang, X. Zhang, J. Chen, W. Zhao, S. Han, G.-H. Nam, M. Sindoro, H. Zhang, Recent advances in ultrathin two-dimensional nanomaterials, Chem. Rev. 117 (2017) 6225–6331, https://doi.org/10.1021/acs.chemrev.6b00558.
[4] A. Kuc, N. Zibouche, T. Heine, Influence of quantum confinement on the electronic structure of the transition metal sulfide TS_2, Phys. Rev. B. 83 (2011) 245213, https://doi.org/10.1103/PhysRevB.83.245213.
[5] X. Zhang, H. Cheng, H. Zhang, Recent progress in the preparation, assembly, transformation, and applications of layer-structured nanodisks beyond graphene, Adv. Mater. 29 (2017) 1701704, https://doi.org/10.1002/adma.201701704.
[6] F. Withers, O. Del Pozo-Zamudio, A. Mishchenko, A.P. Rooney, A. Gholinia, K. Watanabe, T. Taniguchi, S.J. Haigh, A.K. Geim, A.I. Tartakovskii, K.S. Novoselov, Light-emitting diodes by band-structure engineering in van der Waals heterostructures, Nat. Mater. 14 (2015) 301–306, https://doi.org/10.1038/nmat4205.
[7] W.S. Yun, S.W. Han, S.C. Hong, I.G. Kim, J.D. Lee, Thickness and strain effects on electronic structures of transition metal dichalcogenides: 2H- MX_2 semiconductors (M = Mo, W; X = S, Se, Te), Phys. Rev. B. 85 (2012) 033305, https://doi.org/10.1103/PhysRevB.85.033305.
[8] Y. Xia, P. Yang, Y. Sun, Y. Wu, B. Mayers, B. Gates, Y. Yin, F. Kim, H. Yan, One-dimensional nanostructures: synthesis, characterization, and applications, Adv. Mater. 15 (2003) 353–389, https://doi.org/10.1002/adma.200390087.
[9] H. Li, G. Lu, Y. Wang, Z. Yin, C. Cong, Q. He, L. Wang, F. Ding, T. Yu, H. Zhang, Mechanical exfoliation and characterization of single- and few-layer nanosheets of WSe_2 , TaS_2 , and $TaSe_2$, Small 9 (2013) 1974–1981, https://doi.org/10.1002/smll.201202919.
[10] V. Nicolosi, M. Chhowalla, M.G. Kanatzidis, M.S. Strano, J.N. Coleman, Liquid exfoliation of layered materials, Science 340 (80) (2013), https://doi.org/10.1126/science.1226419 1226419–1226419.
[11] Y. Shi, H. Li, L.-J. Li, Recent advances in controlled synthesis of two-dimensional transition metal dichalcogenides via vapour deposition techniques, Chem. Soc. Rev. 44 (2015) 2744–2756, https://doi.org/10.1039/C4CS00256C.
[12] Q. Feng, N. Mao, J. Wu, H. Xu, C. Wang, J. Zhang, L. Xie, Growth of $MoS_{2(1-x)}Se_{2x}$ (x = 0.41–1.00) monolayer alloys with controlled morphology by physical vapor deposition, ACS Nano 9 (2015) 7450–7455, https://doi.org/10.1021/acsnano.5b02506.
[13] a R. Tenne, L. Margulis, M. Genut, G. Hodes, Polyhedral and cylindrical structures of tungsten disulphide, Nature 360 (1992) 444–446, https://doi.org/10.1038/360444a0;
b Y. Feldman, E. Wasserman, D.J. Srolovitz, R. Tenne, High-rate, gas-phase growth of MoS_2 nested inorganic fullerenes and nanotubes, Science 267 (1995) 222–225, https://doi.org/10.1126/science.267.5195.222.
[14] M. Nath, C.N.R. Rao, $MoSe_2$ and WSe_2 nanotubes and related structures, Chem. Commun. (2001) 2236–2237, https://doi.org/10.1039/b107296j.
[15] Y.C. Cheng, Z.Y. Zhu, M. Tahir, U. Schwingenschlögl, Spin-orbit–induced spin splittings in polar transition metal dichalcogenide monolayers, EPL (Europhys. Lett. 102 (2013) 57001, https://doi.org/10.1209/0295-5075/102/57001.
[16] A.-Y. Lu, H. Zhu, J. Xiao, C.-P. Chuu, Y. Han, M.-H. Chiu, C.-C. Cheng, C.-W. Yang, K.-H. Wei, Y. Yang, Y. Wang, D. Sokaras, D. Nordlund, P. Yang, D.A. Muller, M.-Y. Chou, X. Zhang, L.-J. Li, Janus monolayers of transition metal dichalcogenides, Nat. Nanotechnol. 12 (2017) 744–749, https://doi.org/10.1038/nnano.2017.100.
[17] A. Kandemir, H. Sahin, Bilayers of Janus WSSe: monitoring the stacking type: via the vibrational spectrum, Phys. Chem. Chem. Phys. 20 (2018) 17380–17386, https://doi.org/10.1039/c8cp02802h.
[18] H.H. Wu, Q. Meng, H. Huang, C.T. Liu, X.L. Wang, Tuning the indirect-direct band gap transition in the MoS_2-XSe_x armchair nanotube by diameter modulation, Phys. Chem. Chem. Phys. 20 (2018) 3608–3613, https://doi.org/10.1039/c7cp08034d.
[19] Y.F. Luo, Y. Pang, M. Tang, Q. Song, M. Wang, Electronic properties of Janus MoSSe nanotubes, Comput. Mater. Sci. 156 (2019) 315–320, https://doi.org/10.1016/j.commatsci.2018.10.012.
[20] Z.-K. Tang, B. Wen, M. Chen, L.-M. Liu, Janus MoSSe nanotubes: tunable band gap and excellent optical properties for surface photocatalysis, Adv. Theor. Simul. 1 (2018) 1800082, https://doi.org/10.1002/adts.201800082.
[21] R.A. Evarestov, A.V. Kovalenko, A.V. Bandura, A.V. Domnin, S.I. Lukyanov, Comparison of vibrational and thermodynamic properties of MoS_2 and WS_2 nanotubes: first principles study, Mater. Res. Exp. 5 (2018), https://doi.org/10.1088/2053-1591/aadf00.
[22] J. Heyd, G.E. Scuseria, M. Ernzerhof, Hybrid functionals based on a screened Coulomb potential, J. Chem. Phys. 118 (2003) 8207–8215, https://doi.org/10.1063/1.1564060.
[23] R. Dovesi, et al., CRYSTAL17 User's Manual, (2017) http://www.crystal.unito.it/index.php.
[24] S. Grimme, Semiempirical GGA-type density functional constructed with a long-range dispersion correction, J. Comput. Chem. 27 (2006) 1787–1799, https://doi.org/10.1002/jcc.20495.
[25] R.A. Evarestov, A.V. Bandura, V.V. Porsev, A.V. Kovalenko, Phonon spectra, electronic, and thermodynamic properties of WS_2 nanotubes, J. Comput. Chem. 38 (2017) 2581–2593, https://doi.org/10.1002/jcc.24916.
[26] A.V. Bandura, R.A. Evarestov, Structure and stability of SnS_2 -based single- and multi-wall nanotubes, Surf. Sci. 641 (2015) 6–15, https://doi.org/10.1016/j.susc.2015.04.027.
[27] J.C. Conesa, The relevance of dispersion interactions for the stability of oxide phases, J. Phys. Chem. C 114 (2010) 22718–22726, https://doi.org/10.1021/jp109105g.
[28] L. Fernandez Pacios, P.A. Christiansen, Ab initio relativistic effective potentials with spin-orbit operators. I. Li through Ar, J. Chem. Phys. 82 (1985) 2664–2671, https://doi.org/10.1063/1.448263.
[29] M.M. Hurley, L.F. Pacios, P.A. Christiansen, R.B. Ross, W.C. Ermler, *Ab initio* relativistic effective potentials with spin–orbit operators. II. K through Kr, J. Chem. Phys. 84 (1986) 6840–6853, https://doi.org/10.1063/1.450689.
[30] L.A. LaJohn, P.A. Christiansen, R.B. Ross, T. Atashroo, W.C. Ermler, *Ab initio* relativistic effective potentials with spin–orbit operators. III. Rb through Xe, J. Chem. Phys. 87 (1987) 2812–2824, https://doi.org/10.1063/1.453069.
[31] R.B. Ross, J.M. Powers, T. Atashroo, W.C. Ermler, L.A. LaJohn, P.A. Christiansen, *Ab initio* relativistic effective potentials with spin–orbit operators. IV. Cs through Rn, J. Chem. Phys. 93 (1990) 6654–6670, https://doi.org/10.1063/1.458934.
[32] H.J. Monkhorst, J.D. Pack, Special points for Brillouin-zone integrations, Phys. Rev. B. 13 (1976) 5188–5192, https://doi.org/10.1103/PhysRevB.13.5188.
[33] W.J. Schutte, J.L. De Boer, F. Jellinek, Crystal structures of tungsten disulfide and diselenide, J. Solid State Chem. 70 (1987) 207–209, https://doi.org/10.1016/0022-4596(87)90057-0.
[34] R.G. Dickinson, L. Pauling, THE CRYSTAL STRUCTURE OF MOLYBDENITE, J. Am. Chem. Soc. 45 (1923) 1466–1471, https://doi.org/10.1021/ja01659a020.
[35] T. Böker, R. Severin, A. Müller, C. Janowitz, R. Manzke, D. Voß, P. Krüger, A. Mazur, J. Pollmann, Band structure of MoS_2, $MoSe_2$, and α − $MoTe_2$: angle-resolved photoelectron spectroscopy and ab initio calculations, Phys. Rev. B. 64 (2001) 235305, https://doi.org/10.1103/PhysRevB.64.235305.
[36] V.P. Glushko, V.A. Medvedev, L.V. Gurvich, V.S. Yungman, Thermal Constants of Substances Vol 6 Part 2, Wiley, New York, 1999.
[37] R. Gaillac, P. Pullumbi, F.-X. Coudert, ELATE: an open-source online application for analysis and visualization of elastic tensors, J. Phys. Condens. Matter 28 (2016) 275201, https://doi.org/10.1088/0953-8984/28/27/275201.
[38] K.K. Kam, B.A. Parkinson, Detailed photocurrent spectroscopy of the semiconducting group VIB transition metal dichalcogenides, J. Phys. Chem. 86 (1982) 463–467, https://doi.org/10.1021/j100393a010.
[39] P. Raybaud, J. Hafner, G. Kresse, H. Toulhoat, *Ab initio* density functional studies of transition-metal sulphides: II. Electronic structure, J. Phys. Condens. Matter 9 (1997) 11107–11140, https://doi.org/10.1088/0953-8984/9/50/014.
[40] S.S. Grønborg, S. Ulstrup, M. Bianchi, M. Dendzik, C.E. Sanders, J.V. Lauritsen, P. Hofmann, J.A. Miwa, Synthesis of epitaxial single-layer MoS_2 on Au(111), Langmuir 31 (2015) 9700–9706, https://doi.org/10.1021/acs.langmuir.5b02533.
[41] K.F. Mak, C. Lee, J. Hone, J. Shan, T.F. Heinz, Atomically thin MoS_2: a new direct-gap semiconductor, Phys. Rev. Lett. 105 (2010) 136805, https://doi.org/10.1103/PhysRevLett.105.136805.
[42] J. Zhang, S. Jia, I. Kholmanov, L. Dong, D. Er, W. Chen, H. Guo, Z. Jin, V.B. Shenoy, L. Shi, J. Lou, Janus monolayer transition-metal dichalcogenides, ACS Nano 11 (2017) 8192–8198, https://doi.org/10.1021/acsnano.7b03186.
[43] J. Kang, S. Tongay, J. Zhou, J. Li, J. Wu, Band offsets and heterostructures of two-dimensional semiconductors, Appl. Phys. Lett. 102 (2013) 012111, https://doi.org/10.1063/1.4774090.

[44] S. Tongay, J. Zhou, C. Ataca, K. Lo, T.S. Matthews, J. Li, J.C. Grossman, J. Wu, Thermally driven crossover from indirect toward direct bandgap in 2D semiconductors: $MoSe_2$ versus MoS_2, Nano Lett. 12 (2012) 5576–5580, https://doi.org/10.1021/nl302584w.

[45] D. Tonti, F. Varsano, F. Decker, C. Ballif, M. Regula, M. Remškar, Preparation and photoelectrochemistry of semiconducting WS_2 thin films, J. Phys. Chem. B 101 (1997) 2485–2490, https://doi.org/10.1021/jp962550i.

[46] L. Guimarães, A.N. Enyashin, G. Seifert, H.A. Duarte, Structural, electronic, and mechanical properties of single-walled halloysite nanotube models, J. Phys. Chem. C 114 (2010) 11358–11363, https://doi.org/10.1021/jp100902e.

[47] L. Guimarães, A.N. Enyashin, J. Frenzel, T. Heine, H.A. Duarte, G. Seifert, Imogolite nanotubes: stability, electronic, and mechanical properties, ACS Nano 1 (2007) 362–368, https://doi.org/10.1021/nn700184k.

[48] A. Enyashin, G. Seifert, K.D. Sattler (Ed.), HANDBOOK of NANOPHYSICS, Volume IV: Nanotubes and Nanowires, FL: CRC Press, Boca Raton, 201012–1–12–22.

[49] B.L. Gao, S.H. Ke, G. Song, J. Zhang, L. Zhou, G.N. Li, F. Liang, Y. Wang, C. Dang, Structural and electronic properties of zigzag and armchair WSe_2 nanotubes, J. Alloy. Compd. 695 (2017) 2751–2756, https://doi.org/10.1016/j.jallcom.2016.11.197.

[50] B.M. Wong, S.H. Ye, Self-assembled cyclic oligothiophene nanotubes: electronic properties from a dispersion-corrected hybrid functional, Phys. Rev. B. 84 (2011) 075115, https://doi.org/10.1103/PhysRevB.84.075115.

[51] M. Staiger, P. Rafailov, K. Gartsman, H. Telg, M. Krause, G. Radovsky, A. Zak, C. Thomsen, Excitonic resonances in WS_2 nanotubes, Phys. Rev. B. 86 (2012) 165423, https://doi.org/10.1103/PhysRevB.86.165423.

[52] G. Seifert, On the electronic structure of non carbon nanotubes, AIP Conf. Proc. AIP, 2000, pp. 415–418, https://doi.org/10.1063/1.1342545.

[53] E. Scalise, M. Houssa, G. Pourtois, V. Afanas'ev, A. Stesmans, Strain-induced semiconductor to metal transition in the two-dimensional honeycomb structure of MoS_2, Nano Res 5 (2012) 43–48, https://doi.org/10.1007/s12274-011-0183-0.